

Video-based and interference-free axial force detection and analysis for optical tweezers

Sebastian Knust, Andre Spiering, Henning Vieker, André Beyer, Armin Götzhäuser et al.

Citation: *Rev. Sci. Instrum.* **83**, 103704 (2012); doi: 10.1063/1.4757397

View online: <http://dx.doi.org/10.1063/1.4757397>

View Table of Contents: <http://rsi.aip.org/resource/1/RSINAK/v83/i10>

Published by the [American Institute of Physics](#).

Related Articles

Practical axial optical trapping

Rev. Sci. Instrum. **83**, 103106 (2012)

Photophoretic trampoline—Interaction of single airborne absorbing droplets with light

Appl. Phys. Lett. **101**, 131115 (2012)

Auto- and cross-power spectral analysis of dual trap optical tweezer experiments using Bayesian inference

Rev. Sci. Instrum. **83**, 095116 (2012)

Feasibility of encoding Shor's algorithm into the motional states of an ion in the anharmonic trap

J. Chem. Phys. **137**, 064301 (2012)

Polarization-sensitive photophoresis

Appl. Phys. Lett. **101**, 051106 (2012)

Additional information on *Rev. Sci. Instrum.*

Journal Homepage: <http://rsi.aip.org>

Journal Information: http://rsi.aip.org/about/about_the_journal

Top downloads: http://rsi.aip.org/features/most_downloaded

Information for Authors: <http://rsi.aip.org/authors>

ADVERTISEMENT

ORTEC MAESTRO[®] V7 MCA Software

For over two decades, MAESTRO has set the standard for Windows-based MCA Emulation. MAESTRO Version 7.0 advances further:

- New!** Windows 7 64-Bit Compatibility with Connections Version 8
- New!** List Mode Data Acquisition for Time Correlated Spectrum Events
- New!** Improved Peak fit calculations
- New!** Improved graphics handling for multiple displays
- New!** Open spectrum files directly from Windows Explorer
- New!** Improved performance with Job Functions and display updates

MAESTRO continues to be the world's most popular nuclear MCA software in a broad range of applications!



**Now 64-bit
Windows 7
Compatible!**

www.ortec-online.com

Video-based and interference-free axial force detection and analysis for optical tweezers

Sebastian Knust,^{1,a)} Andre Spiering,¹ Henning Vieker,² André Beyer,² Armin Gölzhäuser,² Katja Tönsing,¹ Andy Sischka,¹ and Dario Anselmetti¹

¹*Experimental Biophysics & Applied Nanoscience, Faculty of Physics, Bielefeld University, 33615 Bielefeld, Germany*

²*Physics of Supramolecular Systems, Faculty of Physics, Bielefeld University, 33615 Bielefeld, Germany*

(Received 16 August 2012; accepted 18 September 2012; published online 15 October 2012)

For measuring the minute forces exerted on single molecules during controlled translocation through nanopores with sub-piconewton precision, we have developed a video-based axial force detection and analysis system for optical tweezers. Since our detection system is equipped with a standard and versatile CCD video camera with a limited bandwidth offering operation at moderate light illumination with minimal sample heating, we integrated Allan variance analysis for trap stiffness calibration. Upon manipulating a microbead in the vicinity of a weakly reflecting surface with simultaneous axial force detection, interference effects have to be considered and minimized. We measured and analyzed the backscattering light properties of polystyrene and silica microbeads with different diameters and propose distinct and optimized experimental configurations (microbead material and diameter) for minimal light backscattering and virtually interference-free microbead position detection. As a proof of principle, we investigated the nanopore threading forces of a single dsDNA strand attached to a microbead with an overall force resolution of ± 0.5 pN at a sample rate of 123 Hz. © 2012 American Institute of Physics. [<http://dx.doi.org/10.1063/1.4757397>]

I. INTRODUCTION

The contactless manipulation and measurement of dielectric microparticles with sub-piconewton force resolution¹ is a unique feature of optical tweezers.² To quantify these external forces, the position of the trapped particle has to be determined with both high spatial and temporal resolution preferably in lateral (x and y) and axial (z) directions.³ For lateral force measurements, this can be achieved by collecting the forward or backscattered light of the trapped particle and projecting it onto a position sensitive detector, such as a quadrant⁴ or linear⁵ photo detector. Force measurement in z -direction basically requires an intensity detection of the forward or backscattered light coming from the trapped object.⁶⁻⁸

To collect the forward scattered light, a condenser objective needs to be confocally adjusted to the trapping objective which limits the space between the two lenses and reduces the versatility of the setup.⁹ To overcome this limitation, backscattered light detection can be utilized;^{6,7} however, when operating this system in the vicinity of optical interfaces, disturbing force interference effects occur that can only be partially suppressed with an improved optical setup.⁷

Alternatively, video-based image analysis of the trapped object can be utilized for position detection and tracking but sometimes lacks temporal resolution, which can be overcome by strongly increasing the illumination intensity¹⁰ to reduce exposure time or by limiting the active pixel area to boost data output.

In this paper, we introduce a video-based force detection setup based on a standard CCD camera with a limited bandwidth operating at moderate light illumination with minimal sample heating, which delivers high force resolution in axial direction. Force calibration of the optical trap is realized by Allan variance (AV) algorithm¹¹ and tested with polystyrene (PS) and silica microparticles. As a proof of concept, we analyzed the controlled DNA translocation through a solid-state nanopore (NP) inside a membrane. Moreover, we investigated the axial force response signal of different microparticles when navigating these particles into the vicinity of this weakly reflecting surface. These results are compared to our previous measurements based on backscattered light detection. Furthermore, we show that only video analysis in combination with certain microbead sizes will provide a force signal completely devoid of any force interference effects, for which the backscattered light detection method can only deliver a very limited force signal response.

II. OPTICAL TWEEZERS SETUP

The optical tweezers system is adapted from our previously described backscattered light detection setup^{7,12} (Fig. 1).

Briefly, the P-polarized beam (filled line in Fig. 1(a)) of a 1 W, 1064 nm Nd:YAG-laser (LCS-DTL-322, Laser 2000, Germany) is passing a 1064 nm longpass filter, a polarizing beam splitter cube (Linos, Germany) and is expanded to a diameter of about 9 mm for overfilling the back aperture of the water immersion trapping objective (5.7 mm diameter) with a numerical aperture of 1.2 (UPL-APO60W/IR, Olympus, Japan). Arranged in front, a quarter wave plate

^{a)} Author to whom correspondence should be addressed. Electronic mail: sknust@physik.uni-bielefeld.de.

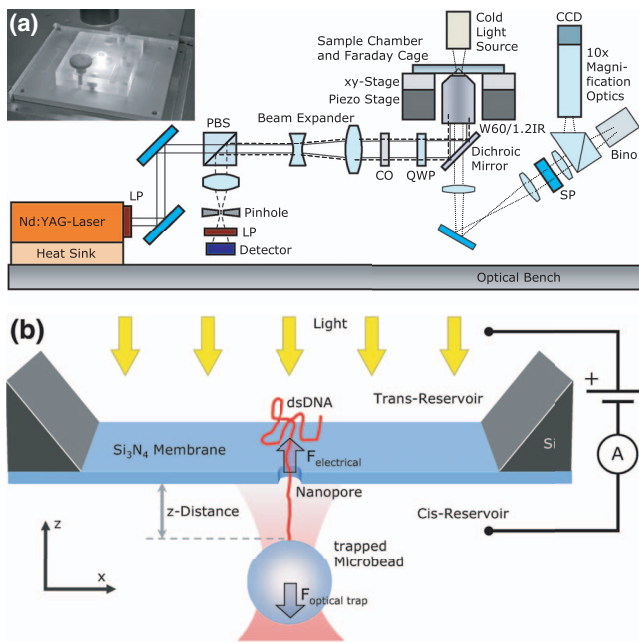


FIG. 1. (a) Quantitative single beam optical tweezers setup with both backscattered light and video-based force detection. Abbreviations: LP: 1064 nm longpass filter; PBS: polarizing beam splitter cube; SP: shortpass filter for visual light; QWP: quarter wave plate; CO: central obstruction filter. Dashed lines indicate backscattered laser light, whereas visible light is indicated as dotted lines. (Inset) Image of the illuminated sample chamber inside the faraday cage (electrical contacting not shown). (b) Detailed view of the Si_3N_4 membrane with nanopore and threaded DNA attached to a trapped microbead. Electrical contacting is shown schematically.

(RM-1/4-1046, Newport, CA) turns the linearly polarized into right-circularly polarized light, which is afterwards reflected by a dichroic mirror (TFP 1064 nm/56°, Laseroptik, Germany). Backscattered laser light (dashed line in Fig. 1(a)) from the trapped particle (now left-circularly polarized) is collected by the trapping objective that turns it into a parallel light beam. The quarter wave plate changes it into linearly S-polarized light and after passing the beam expander, the beam is reflected by the polarizing beam splitter cube and confocally projected (aspherical lens $f = 10$ mm, pinhole diameter of $15 \mu\text{m}$) through a 1064 nm longpass filter onto a photo detector (SD172-11-21-221, Laser Components, Germany).

A central obstruction filter (CO in Fig. 1(a)) placed in the incoming laser light path not only forms a ring-like laser beam profile inducing a higher force constant in z -direction, but considerably reduces disturbing backscattered light from optical interfaces such as a low reflective membrane when performing force measurements on trapped microspheres close to that interface.⁷

For eye and camera safety, two KG5 short pass filters are placed in the path of the visible light (dotted line in Fig. 1(a)).

The custom-built sample chamber encloses a silicon chip with a Si_3N_4 membrane containing a single nanopore.¹² The chamber on each side of that pore is connected to its respective reservoir where a transmembrane voltage can be applied and functionalized microbeads are introduced that can be individually trapped and navigated to the nanopore (Fig. 1(b)). Each reservoir is electrically contacted by an agarose gel and cyanoferrat salt bridge with an embedded platinum wire con-

nected to an Axopatch 200B amplifier (Molecular Devices, CA).

The sample chamber can be coarse-adjusted by a micrometer-precise manual stage and additionally position controlled with nanometer precision by a piezo stage (P-517.3CD, Physik Instrumente, Germany) during all experiments. For illumination, we use a high-power cold light source (KL 2500 LED, Schott, Germany) with an output of 1000 lm at the end of the glass fiber that is installed about 2 cm above the top of the sample chamber (inset of Fig. 1(a)).

III. VIDEO-BASED FORCE ANALYSIS

For video-based force analysis we integrated a CCD camera (Guppy Pro F-031 monochrome, Allied Vision Technologies, Germany) and a custom-built post-magnification with a factor of 10. The focal plane of the camera was aligned to the focal plane of the trap by adjusting the distance until a trapped bead was imaged sharply. Focal imprecision only results in a slightly blurry image of the bead which is not disturbing the analysis significantly, making the analysis robust and reliable. The camera delivers 123 frames per second at a resolution of 492×492 pixels ($5.6 \mu\text{m}$ pixel size) with 14-bit gray scale through Firewire-B connection. Image analysis is completely software based on a CPU with six cores and twelve parallel threads.

Video-based force analysis and particle tracking in lateral direction has been shown in previous papers.^{10,13,14} Usually, these methods involve high speed cameras with limited lateral resolution. Since we want to analyze the axial force acting on a trapped bead in front of a Si_3N_4 membrane, we need to continuously monitor the apparent size of the video-imaged bead. For this purpose, high lateral resolution of the bead's image is mandatory, which is achieved by using a post-magnification in front of the camera resulting in a lateral scale of approximately 9 nm per pixel.

For all measurements, the apparent size of a bead needs to be precisely determined, which is done by searching for specific edges in the single image, as illustrated in Fig. 2(a). First, we manually select a circular region of interest. Then, the strongest falling and rising edges along 360 circular spokes in this circle are determined. If both exceed a certain threshold value and are in the correct relation to each other (which means the falling edge is closer to the bead's center than the rising edge), the middle position between these two edges is calculated (Fig. 2(b)), and a circle is fitted through those points. On demand, to compensate transversal drift, the position of this circle can be used to auto track the region of interest by aligning its center to the center of the circle.

The edge detection is done by utilizing the built-in *IMAQ Spoke 3* function of the NI Vision Development Module 2009 for LabView (National Instruments, TX). We empirically determined the optimal parameters with respect to execution time and noise to be: Kernel Size: 35; Width: 9; Minimum Edge Strength: 0.00; Interpolation Type: Bilinear Fixed; Data Processing Method: Average. As the minimum edge strength is set to zero, the step of comparing the edge strength to the threshold is obsolete. However, it might improve the results

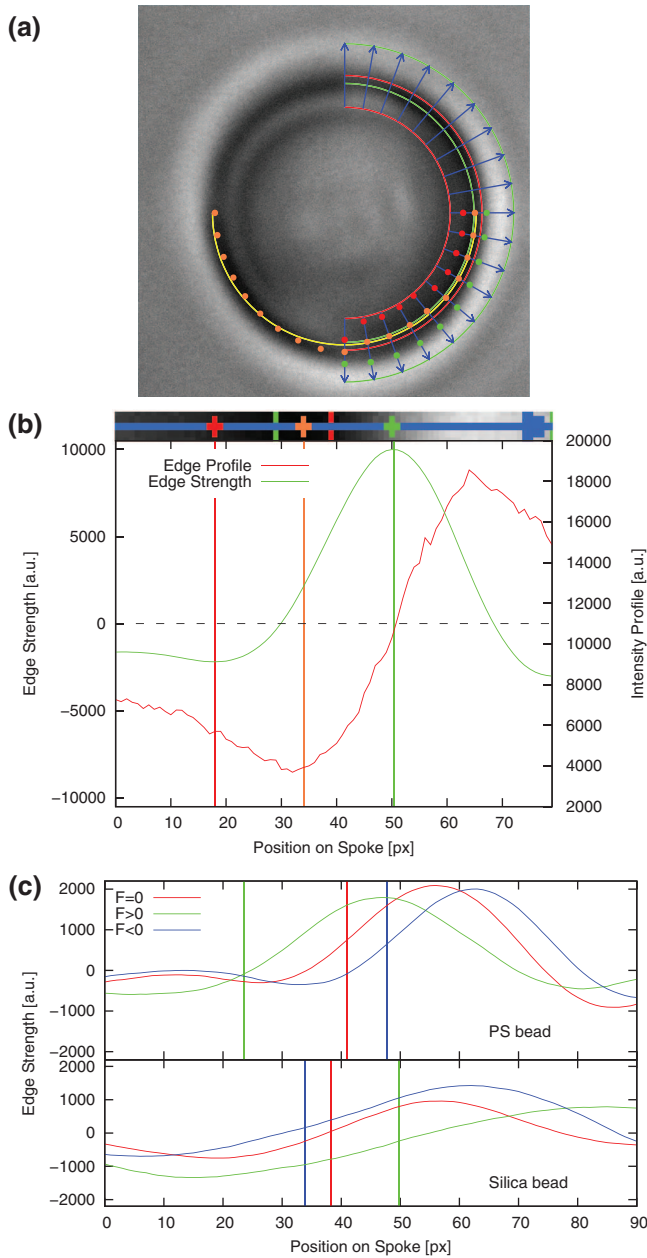


FIG. 2. (a) Still frame of a PS bead with manually selected circular region of interest for falling (red) and rising (green) edge with search spokes (blue). The red and green dots are the recognized falling and rising edges. The orange dots are the resulting mid-points between the two edges, through which the yellow circle is fitted. For clarity, only every tenth spoke with corresponding edges is shown. (b) (Top) Extract of a still frame with region of interest boundaries, spoke, and detected edges. (Bottom) Raw edge profile (red) and calculated edge strength (green) of that profile with marked falling (red) and rising (green) edge position. (c) Edge strength along one spoke for PS (top) and silica (bottom) beads without applied force (red) and with applied positive (green) and negative (blue) force. The middle position between the rising and falling edge is marked by a vertical line.

under different lighting conditions. The LabView source file containing the size detection is available in the supplementary material.²¹

By analyzing six frames in parallel, we are able to analyze the camera images with the maximum frame rate of 123 frames per second in real-time.

IV. FORCE CALIBRATION

Basic force calibration of the optical tweezers was conducted using the drag force via Stokes' law by moving the piezo in z-direction with a specified velocity. As a result, we found that the apparent size of a PS bead decreases, whereas in contrast, the size of a silica bead increases when a positive external force is applied and the bead is axially deflected inside the optical trap (Fig. 2(c)).

It is worth noting that the apparent size of the bead grows minimally when increasing the distance between bead and membrane due to a slight change in the lighting situation. This linear effect is in the order of 0.2% relative size change across the whole piezo stage z-range of 20 μm and can easily be eliminated by a linear correction factor.

The force can now be derived from the calculated apparent radius r as

$$F = k\Delta z = k\beta \times \left(\frac{r}{r_{zf}(z)} - 1 \right). \quad (1)$$

Here, k is the force constant of the optical trap, β is a conversion factor between relative radius change and bead deflection Δz , and $r_{zf}(z)$ is the apparent radius of the bead at zero force.

Because $r_{zf}(z)$ depends on the piezo position as described above, a linear interpolation based on two reference zero force measurements at different piezo positions is included.

For all used PS beads, the conversion factor β is in the order of 10 μm , meaning a 0.025% change of the radius (which is our detection limit) corresponds to a 2.5 nm axial displacement of the bead.

The drag force method can be applied to video-based force analysis, but it yields a calibration error of about 10%. Fitting a Lorentzian function to the thermal noise spectrum is not suitable here due to the rather low sampling rate of the video signal, thus making an alternative method mandatory.

Allan variance is such a method perfectly qualified for low frequency signals.¹¹ It is defined as half the variance of the averaged difference between two consecutive local averaged position samples:

$$\sigma^2(\tau) = \frac{1}{2} \langle (\bar{x}_{\tau,j+1} - \bar{x}_{\tau,j})^2 \rangle, \quad (2)$$

$$\bar{x}_{\tau,j} = \frac{1}{\tau} \int_{\tau(j-0.5)}^{\tau(j+0.5)} dt x(t).$$

Here, $x(t)$ is the bead position, j an integer, and τ the timescale of both the time between consecutive samples and the time over which each sample is being averaged.

AV was primarily used to quantify the performance of generic measurement systems and to quantify the influences of noise and drift;¹⁵ however, it also yields the analytical expression of our trapped bead as a damped harmonic oscillator¹¹ as

$$\sigma_{\text{bead}}^2(\tau) = \frac{2k_B T \gamma}{k^2 \tau} \times \left(1 + \frac{2\gamma}{k\tau} \exp\left[\frac{-k\tau}{\gamma}\right] - \frac{\gamma}{2k\tau} \exp\left[\frac{-2k\tau}{\gamma}\right] - \frac{3\gamma}{2k\tau} \right). \quad (3)$$

Here, $\gamma = 6\pi\eta r$ is the friction coefficient of a microbead with radius r inside a fluid with viscosity η . For the thermal limit $\tau \gg \tau_c$ (with the time-constant $\tau_c = \gamma/k$), the Allan deviation $\sigma_z(\tau)$ of the displacement of a trapped bead reduces to

$$\sigma_z(\tau) = \frac{1}{k} \sqrt{\frac{2k_B T \gamma}{\tau}}, \quad (4)$$

and the force resolution $\sigma_F(\tau) = k\sigma_z(\tau)$ becomes independent of the force constant k .¹⁵

Initially, our recorded video data are in units of relative bead size change with unknown conversion factor β in units of displacement. Fitting $\sigma_z(\tau)/\beta$ (with $\sigma_z(\tau)$ given by Eq. (4)) to the AV of our displacement data delivers the product $k\beta$ —the parameter needed for Eq. (1). In summary, when an external force is acting on the trapped bead the parameter $k\beta$ directly converts the change of the bead size into force. In contrast to the drag force method, the results of this calibration procedure are not accessible in real time but directly after several seconds of data acquisition and analysis. However, because the bead remains in the same position during the AV calibration, this method significantly reduces the possibility to trap dirt particles and suppresses drag force calibration difficulties that may occur when the mobility of the bead in z-direction inside the sample chamber is limited.

To calculate the force constant k separately, the displacement conversion factor β needs to be determined. This is done by immobilizing a bead on the membrane or the sample chamber bottom, moving the bead with the piezo in z-direction through the center of the optical trap that has been switched off, and recording the relative size change $(r(z)/r_{zf}) - 1$. The value of β can then be determined from the slope of a linear fit of the piezo position z versus the relative size change of the bead. β can now be utilized for all trapped beads of the same apparent radius, material, and lighting condition.

V. EXPERIMENTAL PROCEDURE

We use monodisperse streptavidin-coated PS beads (3.05 μm and 3.28 μm nominal diameter, concentration of 0.5% w/v; Spherotech, IL) that were diluted by a factor of 1:2000 in NP-buffer (20 mM KCl and 2 mM Tris/HCl at pH 8.0) and streptavidin-coated silica beads (3 μm nominal diameter, concentration of 2.5% w/v; Spherotech, IL).

Calibration and all experiments were carried out at 21 °C. Temperature control with an IR camera revealed an ambient sample chamber temperature of 25 °C due to intense lighting of the silicon chip. With these conditions, we are able to achieve an AV calibration accuracy of $\pm 5\%$.

For controlled DNA translocation through a NP, Lambda-DNA molecules (16.4 μm contour length; Roche Diagnostics, Germany) were multi-biotinylized at one end and individually attached to a 3.05 μm PS bead.¹² Then, DNA-bead constructs were suspended in NP-buffer, introduced into the sample chamber, trapped, and navigated underneath the NP (Fig. 1(b)).

VI. RESULTS AND DISCUSSION

A. Allan variance calibration

Because various sizes of beads consisting of PS and silica yield qualitatively similar AV graphs, we discuss our results of an exemplary AV graph of a 3.05 μm PS bead trapped with a laser output power of 250 mW (green line in Fig. 3, black error bars). The conversion factor β has been determined as $(9.21 \pm 0.04) \mu\text{m}$. The left ordinate in Fig. 3 displays AV data in nm, and the right ordinate shows the respective relative size change of the trapped bead in percent.

The main section of our data ($\tau < 1$ s) matches very well the theoretical model for the overdamped bead in a harmonic oscillator (Eq. (3), and blue line in Fig. 3), whereas for times larger than several seconds, drift effects deviate the AV results from that model. As both Eq. (3) and the thermal limit (Eq. (4), and red dashed line in Fig. 3) do not deviate within range of our data, a fit of the AV results to the thermal limit is feasible.

Fitting $\sigma_z(\tau)/\beta$ to our data yields the value of $k\beta$ as to be $(106.8 \pm 03) \text{ pN}$, which means a change of the apparent bead size of 0.025% corresponds to a force of 27 fN.

With the predetermined value of β , we calculated k to be $(11.60 \pm 0.02) \text{ pN } \mu\text{m}^{-1}$ (that matches our previous results¹² very well) and the time-constant as $\tau_c = \gamma/k = (2.20 \pm 0.01) \text{ ms}$.

B. The influence of bead size on the interference

Before the implementation of video analysis, backscattered light detection offered the most precise axial force measurements when approaching a weakly reflective optical interface (e.g., a membrane with a NP) because the combination of confocal and spatial filtering by the CO (Fig. 1(a)) delivers a force signal that is only weakly affected by disturbing interference artifacts.^{6,7,16} Thus, it is inevitable to compete the backscatter method against video analysis with regard to the interference effect. For this purpose, a 3.28 μm PS bead (it delivers a sufficient amount of backscattered light⁷) was trapped, calibrated with both detection methods, and approached with a velocity of 200 nm s^{-1} to the 20 nm thin Si_3N_4 membrane, while the force was recorded simultaneously (Fig. 4(a)).

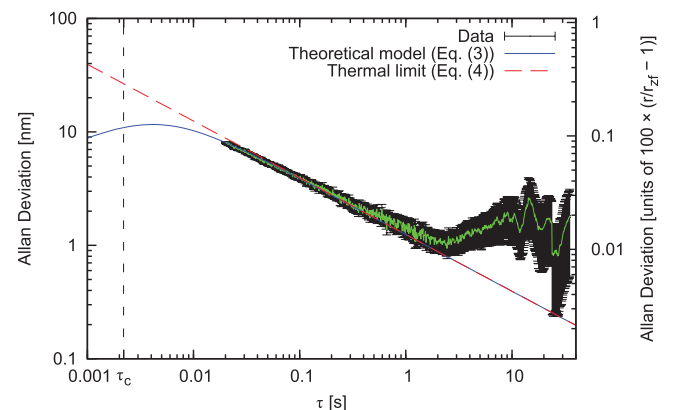


FIG. 3. Exemplary Allan deviation analysis of a trapped 3.05 μm PS bead at 250 mW laser power.

Interestingly, *both* force signals display an almost identical force oscillation of up to ± 1 pN (at 900 mW laser output power). This led us to the conclusion that this phenomenon is not an artifact induced on the photo detector where backscattered light from the trapped bead and (much less) backscattered light from the membrane interfere. Instead, the source of this effect is only located between bead and membrane and can be considered as a standing wave excited by laser light which is backscattered from the membrane and backreflected again from the bead. Bead and membrane can be considered as the “mirrors” of an optical resonator, although their reflectivity is only 0.75% and 1%, respectively. The wave obeys the resonator condition for constructive interference ($j\lambda/2n_w$, where n_w is the refractive index of water) and modulates the position of the trapped bead with respect to the optical trap when varying the distance between bead and membrane—a modulation that both detection methods cannot discriminate from a real external force acting on the bead and deflecting it inside the trap.

The theoretical length for this resonator exciting constructive interference is $j \times 403$ nm, matching our measured length of 409 nm very well (which is the distance between two consecutive force oscillation maxima). The magnitude of the force oscillation depends linearly on the laser power, which is inferred by the fact that the position modulation in terms of nanometer is independent of the laser power, and has an amplitude of up to ± 24 nm for a $3.28 \mu\text{m}$ PS bead.

In contrast, a trapped $3.05 \mu\text{m}$ PS bead exhibits a considerably different behavior since it delivers only about a third of the amount of backscattered light a $3.28 \mu\text{m}$ bead does. Consequently, the resonator’s performance declines by a factor of three, and so do the standing wave and the position modulation of the trapped bead as well. As a result, the oscillation of the force signal measured with video analysis has been diminished to ± 0.3 pN or less (Fig. 4(b)), yielding a very good force signal displaying almost only Brownian noise.

Because of the extremely low amount of backscattered light from the bead, the photo detector’s signal needs to be amplified by a factor of three to maintain its force sensitivity, making the detector more susceptible for backscattered light from the membrane too, since the combination of confocal filtering and the CO can only suppress that backscattered light to a certain amount. Therefore, this force signal is even more affected by that disturbance and exhibits a strong oscillating force artifact of more than ± 2 pN.

As the real size of each trapped bead deviates from its nominal value of 3.05 or $3.28 \mu\text{m}$, a multitude of bead sizes were examined, each with regard to its apparent radius and the respective amount of backscattered light. Figure 4(c) contains two data point clusters attributed to the batch of the smaller (with a radius between 172 and 175 pixels) and larger beads (with a radius between 176 and 178 pixels). Their corresponding amount of backscattered light extends from 0.2 to 0.5 and from 0.7 to 1.0 arbitrary units for $3.05 \mu\text{m}$ and $3.28 \mu\text{m}$ beads, respectively.

The sizes of several beads deviate more significantly from their nominal value, giving us the opportunity to examine a large range of different sizes revealing a rather complex dependency between bead size and amount of backscattered

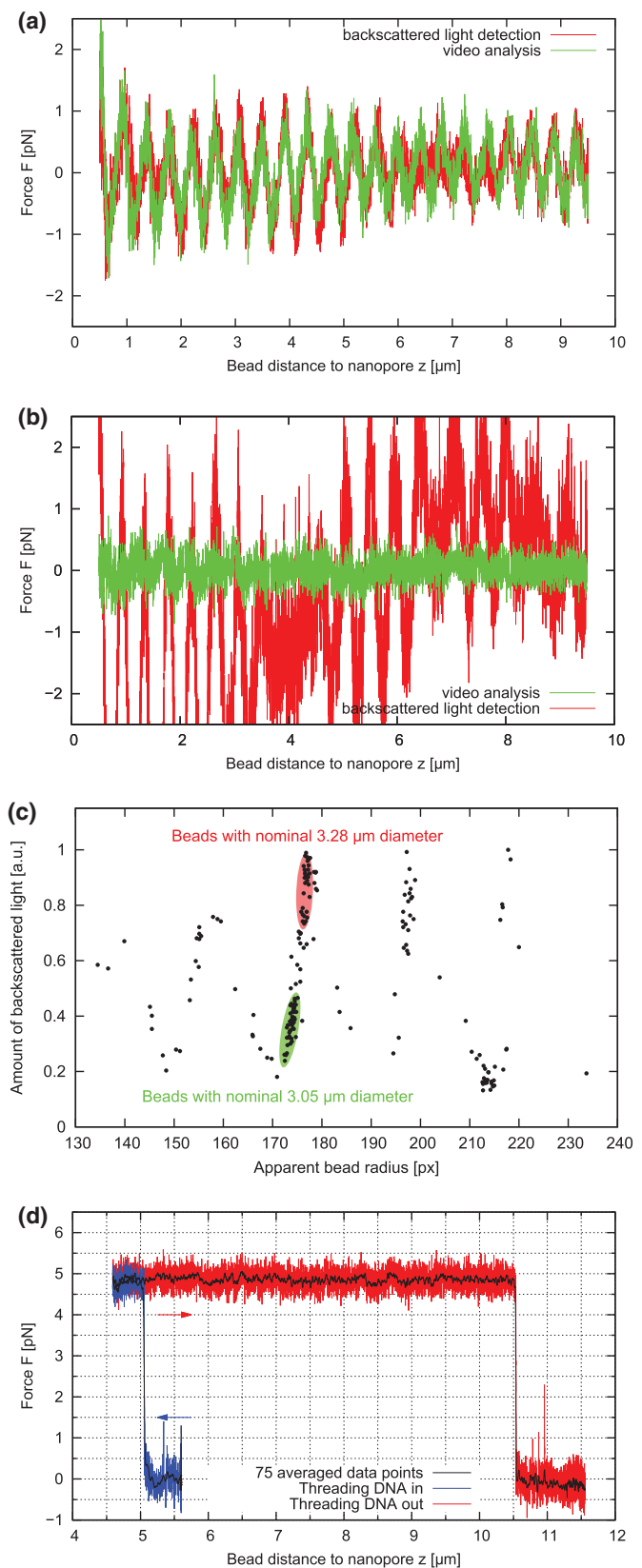


FIG. 4. (a) A $3.28 \mu\text{m}$ bead approaches the membrane, measured both with backscattered light detection and video analysis. (b) A $3.05 \mu\text{m}$ bead approaches the membrane, measured both with backscattered light detection and video analysis. (c) Graph showing the dependency of the amount of backscattered light on the apparent bead size. (d) Controlled dsDNA threading with $3.05 \mu\text{m}$ bead (55 nm pore diameter, applied voltage 50 mV).

light that has been described elsewhere.¹⁷ Extrapolating Fig. 4(c) leads to an optimal PS bead size of 171 pixels corresponding to approximately 3.01 μm .

C. Force measurements during DNA threading

As an appropriate proof of principle, we have measured the small force during a controlled translocation of a single dsDNA strand through a solid state NP with a diameter of 55 nm inside a 20 nm Si_3N_4 membrane that has been drilled as describe before¹⁸ and mounted into the sample chamber. We have introduced freshly prepared bead-DNA constructs into the sample chamber and selected a bead with an apparent radius of 171 pixels, which as shown above is the optimal bead size. Figure 4(d) shows the results of a controlled single-DNA threading event into the NP, when applying a positive voltage of 50 mV to the trans-chamber, before the DNA was completely pulled out of the pore by retracting the bead. While the DNA is inside the pore we have measured an end-to-end distance of this DNA fragment of 10.5 μm and a very constant force signal of 4.9 pN, which is in agreement with force values for large pores.^{19,20} Since the DNA often sticks to the bead, the apparent contour length decreases. Force fluctuations at a sample rate of 123 data points per second were in the range of not more than ± 0.5 pN, whereupon averaging of 75 data points led to extremely low variations of less than ± 0.2 pN with no noticeable force oscillations anymore.

VII. SUMMARY AND CONCLUSION

We presented precise video-based axial force analysis via bead size detection for optical tweezers, which in combination with high magnification allows for an axial displacement resolution of 2.5 nm.

Allan variance was introduced as an alternative force calibration method where fitting a Lorentzian function to the thermal noise spectrum is not possible due to low sampling rates.

The comparison between video-based axial force measurements and backscattered light detection measurements in the vicinity of a weakly reflecting surface led us to the conclusion that interference effects are not artifacts induced on the photo detector but caused by what can be considered a standing wave between the weakly reflecting bead and surface.

We show that beads barely backscattering light exhibit no measurable interference effect in the vicinity of an optical interface. This allows interference-free axial force measurements with the video-based method.

As an exemplary result, we achieved a virtually interference-free axial force resolution of ± 0.5 pN at a sample rate of 123 Hz when threading a single dsDNA molecule into a nanopore.

ACKNOWLEDGMENTS

We gratefully acknowledge helpful discussions with Fabian Czerwinski, Thomas Huser, Zachary J. Smith, Matthias Rief, Cees Dekker, Ulrich F. Keyser, and Gautam Soni. We thank Christoph Pelargus, Karsten Rott, Wiebke Hachmann, and Helene Schellenberg for technical support. This work was financially supported by the Collaborative Research Center SFB 613 from the Deutsche Forschungsgemeinschaft (DFG).

- ¹J. R. Moffitt, Y. R. Chemla, S. B. Smith, and C. Bustamante, *Annu. Rev. Biochem.* **77**, 205 (2008).
- ²A. Ashkin, J. M. Dziedzic, J. E. Bjorkholm, and S. Chu, *Opt. Lett.* **11**, 288 (1986).
- ³K. C. Neuman and S. M. Block, *Rev. Sci. Instrum.* **75**, 2787 (2004).
- ⁴F. Gittes and C. F. Schmidt, *Opt. Lett.* **23**, 7 (1998).
- ⁵J. Huisstede, K. van der Werf, M. Bennink, and V. Subramaniam, *Opt. Express* **13**, 1113 (2005).
- ⁶U. F. Keyser, J. van der Does, C. Dekker, and N. H. Dekker, *Rev. Sci. Instrum.* **77**, 105105 (2006).
- ⁷A. Sischka, C. Kleimann, W. Hachmann, M. M. Schafer, I. Seuffert, K. Tönsing, and D. Anselmetti, *Rev. Sci. Instrum.* **79**, 63702 (2008).
- ⁸C. Deufel and M. D. Wang, *Biophys. J.* **90**, 657 (2006).
- ⁹M. J. Lang, C. L. Asbury, J. W. Shaevitz, and S. M. Block, *Biophys. J.* **83**, 491 (2002).
- ¹⁰O. Otto, F. Czerwinski, J. L. Gornall, G. Stober, L. B. Oddershede, R. Seidel, and U. F. Keyser, *Opt. Express* **18**, 22722 (2010).
- ¹¹B. M. Lansdorp and O. A. Saleh, *Rev. Sci. Instrum.* **83**, 025115 (2012).
- ¹²A. Sischka, A. Spiering, M. Khaksar, M. Laxa, J. König, K.-J. Dietz, and D. Anselmetti, *J. Phys.: Condens. Matter* **22**, 454121 (2010).
- ¹³O. Otto, J. L. Gornall, G. Stober, F. Czerwinski, R. Seidel, and U. F. Keyser, *J. Opt.* **13**, 44011 (2011).
- ¹⁴O. Otto, C. Gutsche, F. Kremer, and U. F. Keyser, *Rev. Sci. Instrum.* **79**, 23710 (2008).
- ¹⁵G. M. Gibson, J. Leach, S. Keen, A. J. Wright, and M. J. Padgett, *Opt. Express* **16**, 14561 (2008).
- ¹⁶A. Jonáš, P. Zemánek, and E.-L. Florin, *Opt. Lett.* **26**, 1466 (2001).
- ¹⁷V. Bormuth, A. Jannasch, M. Ander, C. M. van Kats, A. van Blaaderen, J. Howard, and E. Schäffer, *Opt. Express* **16**, 13831 (2008).
- ¹⁸A. Spiering, S. Getfert, A. Sischka, P. Reimann, and D. Anselmetti, *Nano Lett.* **11**, 2978 (2011).
- ¹⁹S. van Dorp, U. F. Keyser, N. H. Dekker, C. Dekker, and S. G. Lemay, *Nat. Phys.* **5**, 347 (2009).
- ²⁰M. van den Hout, I. D. Vilfan, S. Hage, and N. H. Dekker, *Nano Lett.* **10**, 701 (2010).
- ²¹See supplementary material at <http://dx.doi.org/10.1063/1.4757397> for the LabView source file containing the size detection.